Journal of Nanostructure in Chemistry (2019) 9:163–173
https://doi.org/10.1007/s40097-019-0307-8

ORIGINAL RESEARCH

Structural, microstructural and magnetic properties of sol–gel-synthesized novel $BaZrO_3$–$CoFe_2O_4$ nanocomposite

Pankaj P. Khirade[1]

Received: 20 March 2019 / Accepted: 28 May 2019 / Published online: 15 June 2019

Abstract

A novel $0.5(BaZrO_3)$–$0.5(CoFe_2O_4)$ (BZ–CF) nanocomposite ceramics has been synthesized using sol–gel autocombustion and mixing technique. The structural analysis was carried out using X-ray diffraction (XRD) technique. The XRD pattern shows mixed perovskite and spinel ferrite phases with simple cubic structure for the BZ–CF nanocomposite. The calculated average crystallite size of the samples varies of the order of the nanoregime. The lattice parameter (a) and other structural parameter were obtained using XRD data and it is found that the structural data of pure parent ceramics were in the reported range. The surface morphology of grains of the present samples was examined using field emission scanning electron microscopy (FESEM) and transmission electron microscopy (TEM). The FESEM images show spherical particles with average grain size in the nanometer range. Compositional stoichiometry was confirmed by energy dispersive spectrum (EDX) analysis. Fourier-transform infrared spectra (FTIR) of barium zirconate (BZ) and cobalt ferrite (CF) confirmed the perovskite and spinel ferrite structure, respectively. However, the FTIR spectrum of BZ–CF nanocomposite confirmed the change in crystal structure due to mixed phases. The M–H curves recorded at room temperature using pulse field hysteresis loop tracer technique exhibits a weak hysteresis loop for BZ–CF nanocomposite, perfectly diamagnetic nature for BZ nanoceramics, and typical ferromagnetic hysteresis loop for pure CF nanoceramics.

✉ Pankaj P. Khirade
pankajkhirade@gmail.com

[1] Department of Physics, S.B.E.S. College of Science, Aurangabad, Maharashtra 431001, India

Graphic abstract

The graphical abstract presenting the synthesis process, FESEM micrograph and M–H plot for BZ–CF nanocomposite.

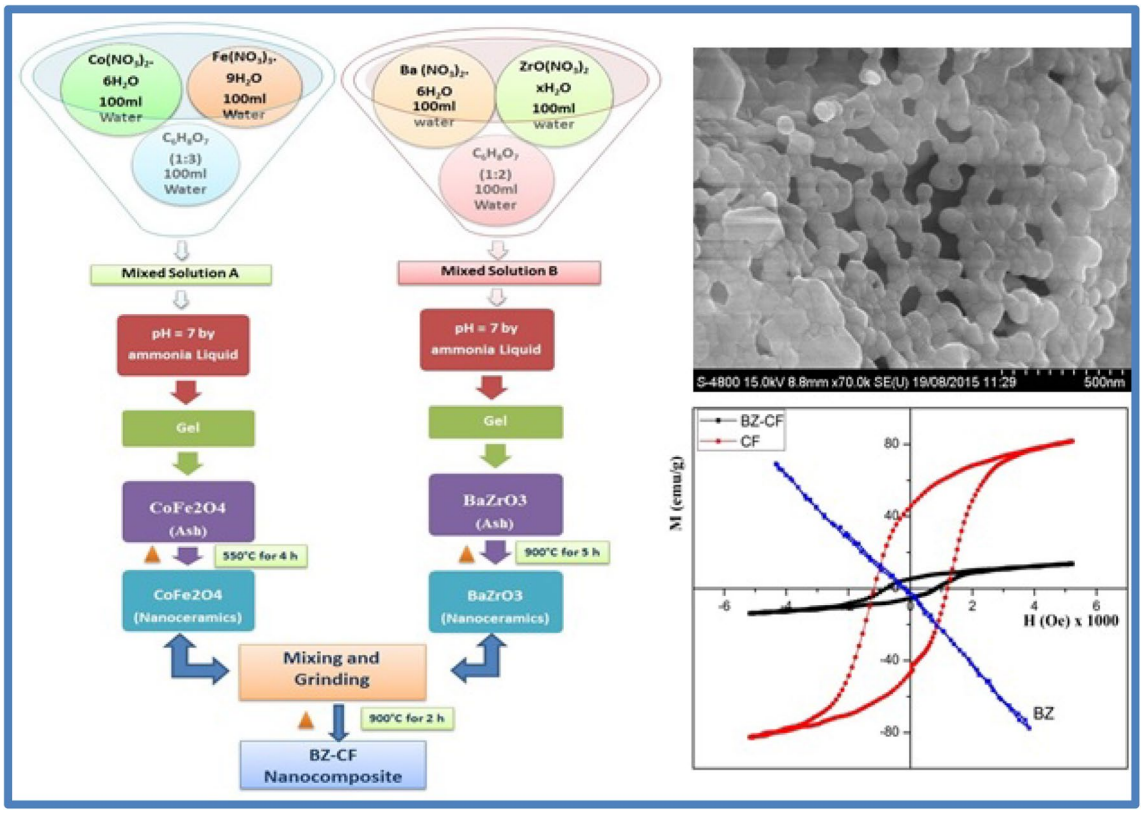

Keywords Nanocomposite · Sol–gel autocombustion · Barium zirconate · Cobalt ferrite · Nanoceramics

Introduction

The accomplishment of new requirements of the tomorrow's society and for innovative technological advancement, there is a consistent quest for novel materials with better than ever properties. A composite material is a material fabricated from two or more constituent materials with considerably different physical or chemical properties that, once combined, produce a material with characteristics different from the parent source materials [1].

In the past decade, renewed interest has been dedicated to perovskites (ABO_3) and spinels (AB_2O_4) because of the opportunity of combining these oxides in composite structures to obtain multifunctional materials [2–4]. Composite powders merging perovskites and spinels have been usually prepared by the mixture method [5, 6]. Composites with nanodimensions are desirable for the synthesis of materials with unique or improved properties.

Perovskite-structured electroceramics materials are worthy materials used for several applications such as high-efficiency solar cells, fuel cells, catalysis, capacitors, superconductors, electrochemical sensing, underwater devices, spintronics devices, etc. [7–10]. They retain some diverse properties, viz., multiferroic, thermoelectric, dielectrical, and optical properties [11]. Barium zirconate ($BaZrO_3$) is of great engineering and technological interest due to their striking characteristics like high melting point, huge thermal resistivity, excellent mechanical stability, outstanding structural reliability under extreme thermal conditions, high protonic conductivity, pyroelectric properties [12, 13]. Nowadays, barium zirconate sputtering targets can be used in the chemical vapor deposition (CVD) and physical vapor deposition (PVD) techniques [14, 15]. Furthermore, the extraordinary dielectric properties of $BaZrO_3$ ceramics recommend it as a favorable material for microwave and wireless communication applications [16, 17].

Ferrites are magnetic ceramics of great importance in countless scientific and technological applications on account of their numerous electrical, magnetic, and dielectric properties. In the class of ferrites, spinel ferrites with chemical formula MFe_2O_4 (where, M represents divalent ions of the transition metal elements such as Co^{2+}, Ni^{2+},

Zn^{2+}, Mg^{2+}, etc.) are industrially leading magnetic materials due to their outstanding electromagnetic properties [18]. The high electrical resistivity, low eddy current and dielectric loss, high saturation magnetization, high permeability, good chemical stability, easiness of preparation, low cost fabrication, etc., are the remarkable features of spinel ferrites [19]. Cobalt ferrite ($CoFe_2O_4$) nanoparticles have received increasing consideration because of their high coercivity at room temperature, high curie temperature, moderate saturation magnetization, superparamagnetism that mark them ideal materials for high-density information storage devices, biomedical nanotechnology, and medicine applications [20–23].

In recent years, materials and composites characterized with submicron and nanosized structures have attracted wide attention due to their unusual mechanical, electrical, optical, and magnetic properties [24, 25]. The nanoceramic materials composed of nanosize crystallites display enhanced performances in comparison to conventionally fabricated bulk grained materials. The composite materials can be manufactured by merging ferrite and ferroelectric ceramics exhibiting magnetoelectric property are used for scientific and technological applications due to multiferroic properties [26, 27].

While synthesizing the nanoparticles, the coarseness and aggregation of the nanocrystals at higher temperature are the critical obstructions for most of the synthesis technique [28]. To overcome these obstacles, efforts have been made by dispersing nanoparticles in matrix-alike silica [29], glass [30], resin [31], and polymers [32].

The disadvantages of the conventional ceramic method such as reduced dispersion of the constituents, high porosity, and large particle size can be fixed with the help of wet chemical sol–gel autocombustion technique [27]. A sol–gel method has certain benefits as it has a precise control over the composition, purity, and superior homogeneity at a molecular level, less energy consumption, low cost, comparatively low annealing time, ecofriendly, etc. [33].

The motivation behind producing $0.5(BaZrO_3)$–$0.5(CoFe_2O_4)$ (BZ–CF) nanocomposite material is that this material is expected to be soft magnetic and have high DC electrical resistivity, excellent mechanical and thermal stability, high dielectric constant, and improved optical properties. These diverse properties inspired me to work on structural, microstructural, electrical, dielectrical, magnetic properties of BZ–CF nanocomposite ceramics. The obtained material can be suitable for fabrication of spintronics and microwave devices.

In this article, I report the synthesis, structural, microstructural, and magnetic properties of $0.5(BaZrO_3)$–$0.5(CoFe_2O_4)$ nanocomposite for the first time. The results are compared with the parent barium zirconate and cobalt ferrite nanoceramics.

Experimental

Materials

For the synthesis of $0.5(BaZrO_3)$–$0.5(CoFe_2O_4)$ nanocomposite, analytical grade (AR) barium nitrate hexahydrate ($Ba(NO_3)_2{\cdot}6H_2O$, 99%), zirconium (IV) oxynitrate ($ZrO(NO_3)_2{\cdot}H_2O$, 99.9%), cobalt nitrate hexahydrate ($Co(NO_3)_2{\cdot}6H_2O$, 99%), ferric nitrate nonahydrate ($Fe(NO_3)_2{\cdot}9H_2O$, 99%), citric acid ($C_6H_8O_7$, 99.57%), and ammonium hydroxide (NH_4OH, 99%) purchased from S.D. Fine chemicals Ltd. (Mumbai) were used without additional purification.

Synthesis of $BaZrO_3$ (BZ) nanoceramics

$BaZrO_3$ nanoceramics were synthesized using sol–gel autocombustion technique. Barium nitrate hexahydrate and zirconium (IV) oxynitrate were used as the precursors. The metal nitrate (barium nitrate) to fuel (citric acid) ratio was taken as 1:2. The precursor solutions were mixed and the resultant mixture was subjected to continuous stirring and heating at 80–90 °C on a magnetic stirrer until a homogenous mixture was obtained. Ammonia was added into the solution till the mixture became neutral (pH = 7). Uninterrupted heating of 110 °C initiates the formation of a continuous network of gel. Resulting gels were heated further; after 4 h the fast flameless autocombustion reaction with the exhaust of fumes forming burnt ash takes place. The obtained powders were ground finely in an agate mortar and were annealed at 900 °C for 5 h in a muffle furnace to complete different levels of crystallinity and to get the required $BaZrO_3$ powder.

Synthesis of $CoFe_2O_4$ (CF) nanoparticles

$CoFe_2O_4$ nanoparticles were synthesized using sol–gel autocombustion technique. Analytical grade (AR) chemicals such as cobalt nitrate, ferric nitrate, and citric acid (fuel) were used for the synthesis. The metal nitrates to fuel ratio was taken as 1:3. Ammonia solution was added to maintain the pH 7. The temperature required for the synthesis of cobalt ferrite nanoparticles was low that is around 110 °C. The as-synthesized powder is sintered at 550 °C for 4 h.

Synthesis of $0.5(BaZrO_3)$–$0.5(CoFe_2O_4)$ BZ–CF nanocomposite

The prepared fine powders of cobalt ferrite and barium zirconate were mixed thoroughly and ground in molar proportion using pestle mortar above 1 h. The mixture was then

sintered at 900 °C for 2 h, and then used for further investigations. The flowchart of the sol–gel synthesis of BZ–CF nanocomposite is presented in Fig. 1.

Characterizations

The structural properties of the samples are studied by PANalytical X'pert Pro diffractometer using the Cu–Kα radiation ($\lambda = 1.54182$ Å) at room temperature. The samples were mixed with 8–10% polyvinyl alcohol (PVA) as a binder and pressed into the desired cylindrical shape pellet using a uniaxial hydraulic press at 12 MPa pressure. The pressed compact pellets were sintered at 900 °C for 2 h and used for bulk density measurement employing the Archimedes' principle. Microstructures of the sintered samples were obtained by field emission gun scanning electron microscope (FESEM, Hitachi Model-S-4800) operated at 15 kV. The transmission electron microscope (TEM, Philips Model-CM 200) operating at 20–200 kV was employed to determine the accurate particle size. The elemental composition is determined using energy dispersive X-ray analysis (EDX). The Fourier-transform infrared spectra (FTIR) were recorded in the region 4000–400 cm^{-1} using Perkin–Elmer spectrum 100 spectrophotometer using KBr as a reference material to determine the vibrational structures of the prepared materials.

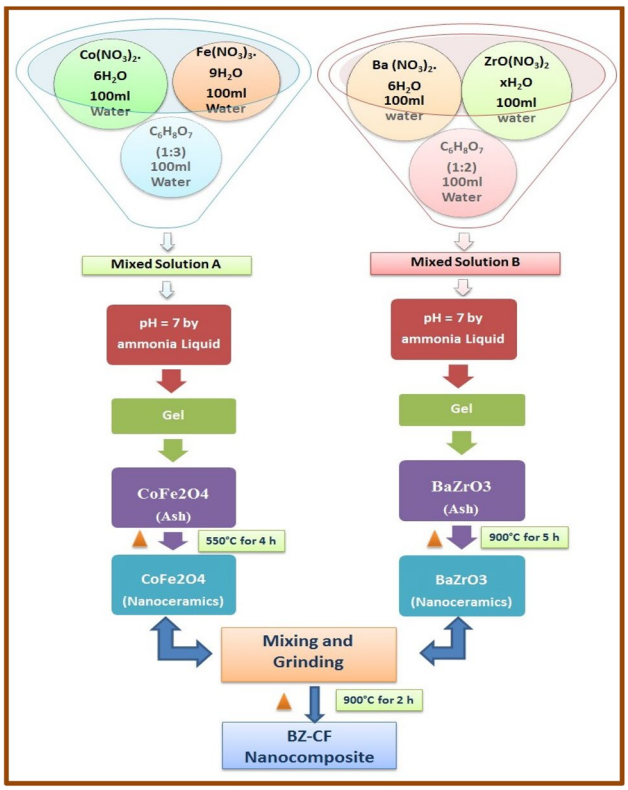

Fig. 1 The flowchart of synthesis of BZ–CF nanocomposite

The magnetic hysteresis loops were measured using pulse field hysteresis loop technique (Magnata Company) at room temperature.

Results and discussion

Structural studies of BZ–CF nanocomposite, BZ, and CF nanoceramics under investigation were carried out using X-ray diffraction (XRD) technique. Figure 2a gives XRD pattern of the pure BZ nanoceramics. All the observed diffraction peaks can be indexed to perovskite $BaZrO_3$ phase with a cubic perovskite structure. The peak position of the $BaZrO_3$ phase agrees well with standard JCPDS: 06-0399 data that has a *Pm3m* space group [34]. The minor peak (indexed by asterisk * mark) is assigned to the orthorhombic barium carbonate ($BaCO_3$) phase (JCPDS: 05-0378) with a *Pmcn* space group. The leading (110) diffraction plane relates to the periodic arrangement of the dodecahedral (BaO_{12}) and octahedral (ZrO_6) sites [35].

All the peaks in the XRD pattern of pure CF sample, Fig. 2b were indexed using Bragg's law and the reflections (220), (311), (222), (400), (422), (511), and (440) showed the development of single phase cubic spinel structure, space group *Fd3 m*, and well matches with the JCPDS-22-1086 data [36].

Figure 2c shows the XRD pattern of the BZ–CF nanocomposite. It is clearly seen that two phases, viz., perovskite and ferrite phases can be clearly identified in the nanocomposites. A very slight amount of $BaCO_3$ phases other than BZ perovskite and CF spinel ferrite was observed.

The lattice cell parameter of BZ, CF ceramics, and BZ–CF nanocomposite was determined from XRD analysis with an accuracy of ± 0.002 Å using relations (1) [37]

$$\frac{1}{d^2} = \frac{h^2 + k^2 + l^2}{a^2}, \tag{1}$$

where a is the lattice parameter, d the interplanar spacing, and (hkl) are Miller indices. For pure $BaZrO_3$ and $CoFe_2O_4$, lattice parameter was found to be 4.1809 Å and 8.3760 Å, respectively, which is in a good agreement with the reported values [38, 39]. The data on lattice parameter for the BZ–CF nanocomposites are given in Table 1.

The materialization of perovskite structure of BZ can be predicted theoretically by computing the tolerance factor (t') suggested by Goldschmidt and it is found to be 1.0441 [40].

The average particle size (t) was estimated using the Debye–Scherrer formula using XRD data and is obtained to be in the nanometer range for all the samples. Additional crystalline parameters like X-ray density (d_x), unit cell volume (V), porosity ($\%P$), etc. have been calculated from XRD data and their values are revealed in Table 1.

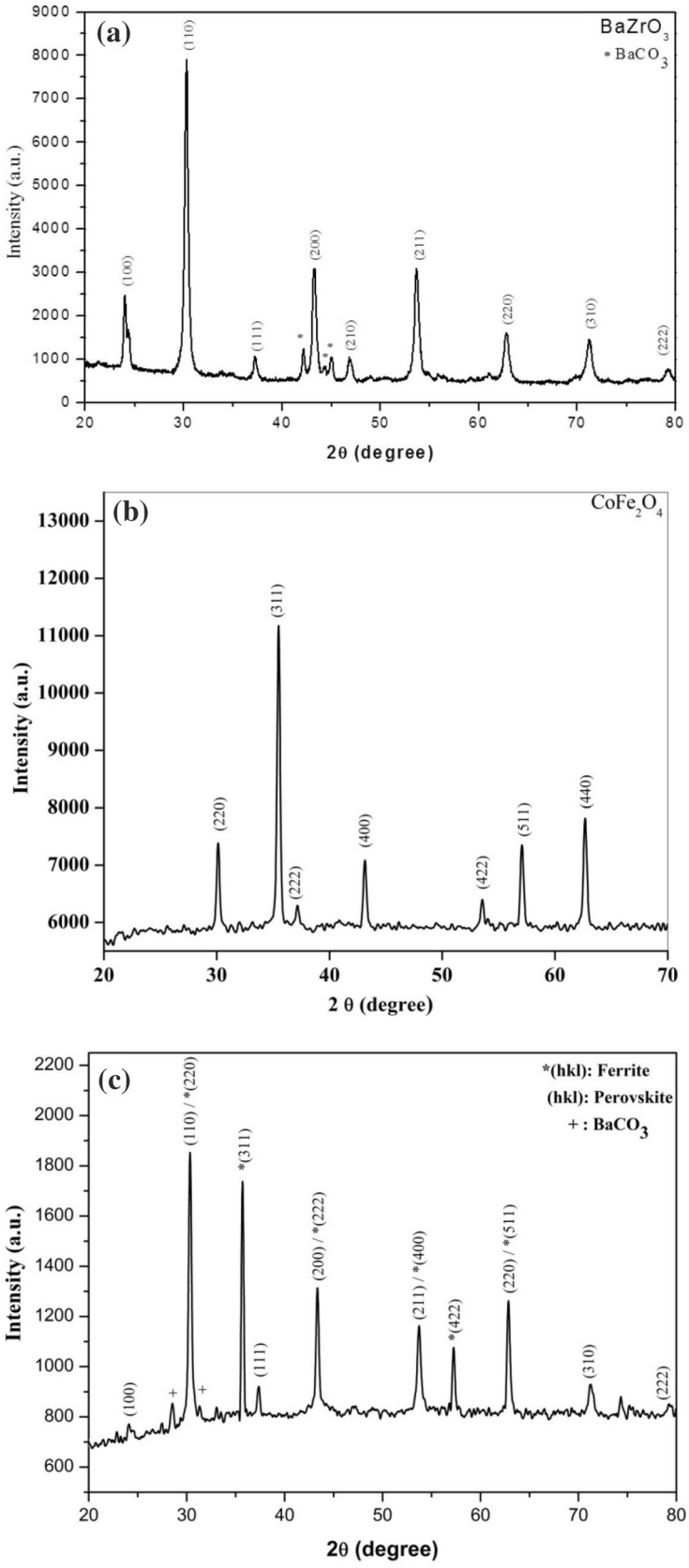

Fig. 2 Room temperature XRD patterns of **a** $BaZrO_3$ nanoceramics **b** $CoFe_2O_4$ nanoferrite and **c** $0.5(BaZrO_3)$–$0.5(CoFe_2O_4)$ nanocomposite

Table 1 Lattice parameter (a), unit cell volume (V), X-ray density (d_x), bulk density (d_B), porosity (P %), molecular weight, average crystallite size (t), and grain size (G) of BZ, CF nanoceramics, and BZ–CF nanocomposite

Sample	a (Å)	V (Å^3)	d_x (g/cm^3)	d_B (g/cm^3)	P (%)	Mol. wt. (g/mol)	t (nm)	G (nm)
BZ	4.1809	73.080	6.2828	5.7029	9.230	276.54	18.86	47
CF	8.3760	587.60	5.3042	3.6380	31.41	234.61	34.52	74
BZ–CF	BZ = 4.1859 CF = 8.382	BZ = 73.08 CF = 589.90	5.6852	4.4352	21.98	255.57	35.12	92

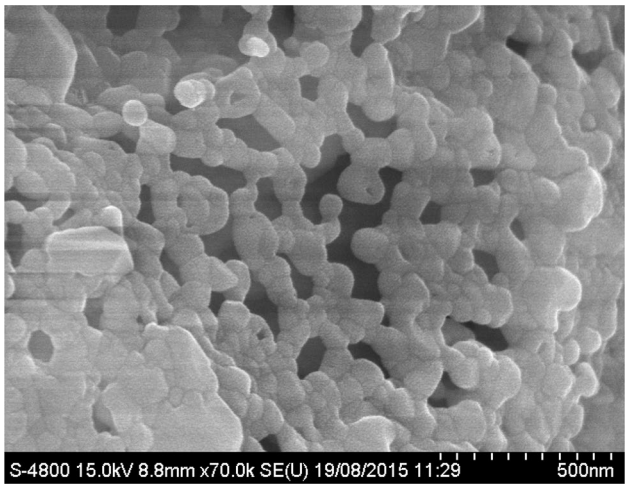

Fig. 3 FESEM micrograph of BZ–CF nanocomposite

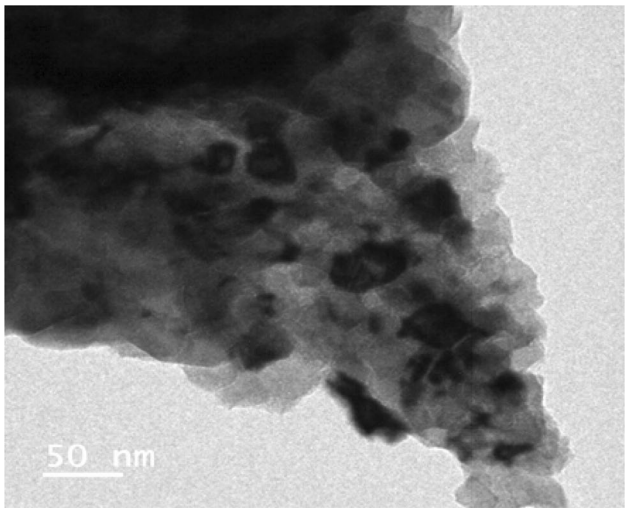

Fig. 4 TEM image of BZ–CF nanocomposite

The X-ray density is an influential parameter used to characterize any material in any form, viz., bulk, thin films or powder and its ability also to explore any changes in the crystal structure of the crystalline material. It is a well admitted fact that the properties of polycrystalline ceramics are dependent on density. The value of the unit cell volume and molecular weight was used to determine the X-ray density of the prepared samples and their values are given in Table 1 [41].

The bulk density (d_B) of the sintered pellets was measured using the Archimedes' method using water as solvent ($\rho = 0.997$ g/cm^3) [42]. The values of bulk density are given in Table 1. The values of bulk densities are found to be lesser than that of X-ray densities. The values of X-ray density and bulk density of BZ–CF nanocomposite are found to be in intermediate of that, of parent materials (BZ and CF). The large values of porosity are attributed to the agglomeration of particles during the combustion synthesis.

FESEM micrograph of typical BZ–CF nanocomposite sintered at 900 °C is shown in Fig. 3. It can be noticed from FESEM image that the synthesized nanoparticles were spherical in morphology with some degree of agglomeration. The FESEM micrograph agrees with the XRD data confirming the grain size in nanoscale. The FESEM image demonstrating a very good homogeneity resulted from this synthesis method. The values of grain size (G) are given in Table 1. The average grain size of BZ–CF nanocomposite ceramics is found to be greater than pure BZ and CF nanoceramics.

The transmission electron microscope (TEM) image of the sample was analyzed to confirm the shape and nanocrystalline size of the prepared nanocomposite. TEM study verified that sphere-shaped, unbroken nanocrystalline powders were successfully synthesized. The TEM micrographs of BZ–CF nanocomposite powder sample are shown in Fig. 4. Cubical shaped agglomerated particles with spherical shape particles were observed. The obtained average crystallite size of the prepared nanocomposite from TEM was in the range of ~ 36 nm. The TEM particle size matches with that calculated from XRD data using Debye–Scherrer formula.

The elemental compositional analysis of synthesized samples was studied by energy dispersive X-ray (EDX) spectrometer attached with FESEM. EDX pattern of BZ–CF nanocomposite is shown in Fig. 5. The EDX pattern reveals the presence of Ba^{2+}, Co^{2+}, Zr^{4+}, Fe^{3+}, and O^{2-} elements in the proper proportions suggesting that predictable stoichiometry was preserved in the prepared sample with an error of 1–2%. Table 2 gives the elemental weight percentage

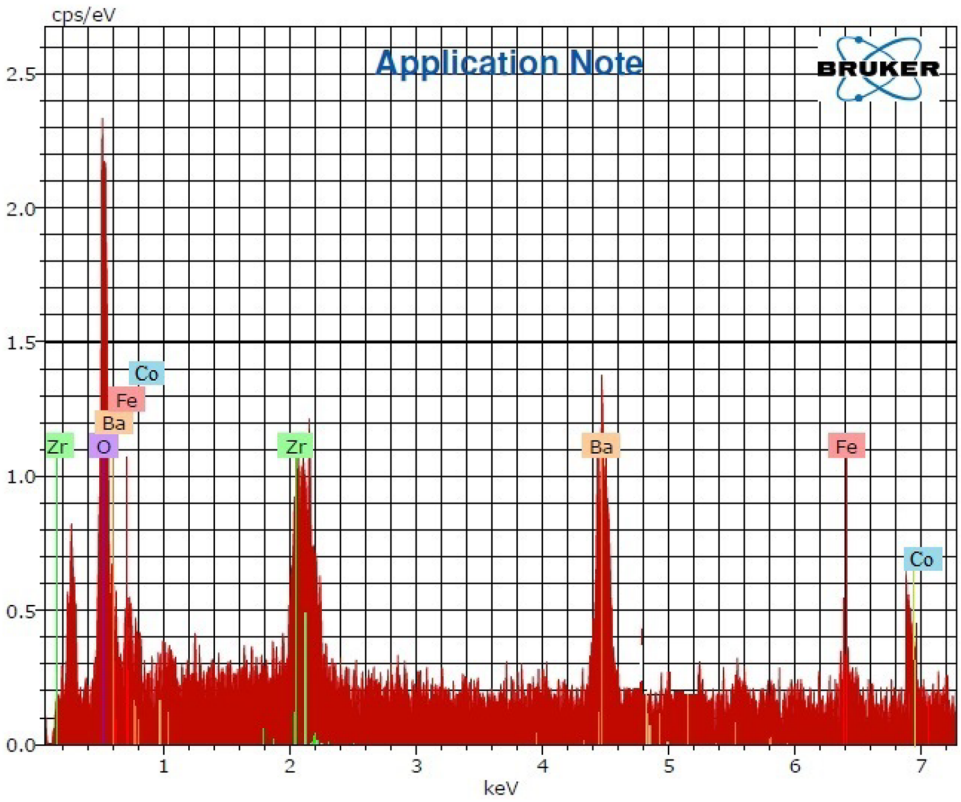

Fig. 5 EDX spectra of BZ–CF nanocomposite

Table 2 Elemental weight percentage (wt %) and atomic percentage (at %) of BZ, CF nanoceramics, and BZ–CF nanocomposite

Sample	Ba		Zr		Fe		Co		O	
	wt %	at %	wt %	at %	wt %	at %	wt %	at %	wt %	at %
BZ	44.71	12.52	22.92	9.66	–	–	–	–	32.37	77.82
CF	–	–	–	–	51.62	25.98	23.62	13.12	24.76	60.9
BZ–CF	30.04	7.32	16.98	7.33	21.02	19.38	13.26	6.16	18.70	59.81

(wt%) and atomic percentage (at%) of BZ, CF nanoceramics, and BZ–CF nanocomposite.

FTIR spectra of the BZ–CF nanocomposite along with their parents are shown in Fig. 6a–c. The FTIR spectrum of pure BZ (Fig. 5a) shows a major band around 560 cm^{-1} which can be attributed to stretching vibrations of metal–oxygen (Zr–O) octahedra. This noticeable absorption bands correspond to metal–oxygen stretching vibrations at the B site of ABO_3 perovskite compounds [43]. The position of this absorption bands mainly depend upon the nature of the cations present and also on the bond lengths. The FTIR spectrum of pure CF (Fig. 6b) shows two major absorption bands found in the range of 700–500 cm^{-1} and 450–400 cm^{-1}. These two noticeable bands correspond to spinel ferrites as recommended by Waldron [44]. The higher frequency band (ν_1) and lower frequency band (ν_2) are caused by metal–oxygen vibration in octahedral (B) site. The small bands correspond to stretching and bending vibrations of H–O–H bonds, indicating the presence of absorbed water.

The FTIR spectrum of BZ–CF nanocomposite (Fig. 6c) shows major bands at around 440 cm^{-1}, 770 cm^{-1} which are caused by the mix phases of perovskite and spinel ferrite phases. The small bands around 1630 cm^{-1}, 2036 cm^{-1}, and 3455 cm^{-1} are ascribed to the stretching and bending of the O–H bond. The FTIR analysis results are analogous to the results obtained from XRD [45].

To examine the magnetic properties, M–H hysteresis loops were recorded using pulse field hysteresis loop technique operated at an applied magnetic field of 10 kOe at room temperature. Figure 7 presents the M–H loops at room temperature for pure BZ, CF nanoceramics, and BZ–CF nanocomposite. The pure CF shows a typical ferromagnetic nature with coercivity (Hc) of 1172.3 Oe. However, the BZ–CF nanocomposite shows non-linearity with a small coercive field, i.e., 809.5 Oe. The pure BZ sample does not show any hysteresis loop as it is diamagnetic in nature. It reveals that the pure BZ sample is intrinsic diamagnetic as reported in the literature [46]. The values of other magnetic

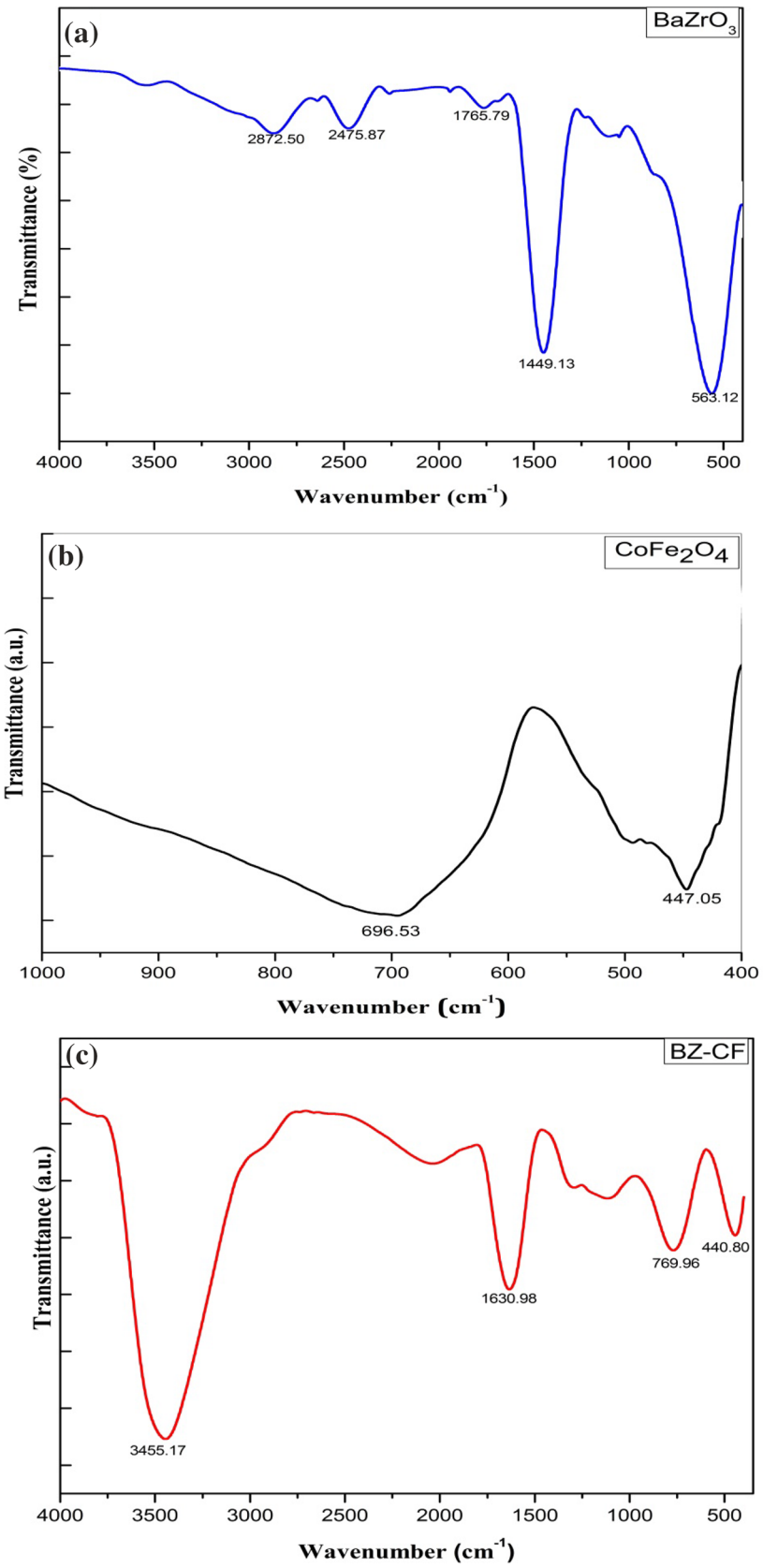

Fig. 6 FTIR spectra of **a** BZ nanoceramics **b** CF nanoceramics **c** BZ–CF nanocomposite

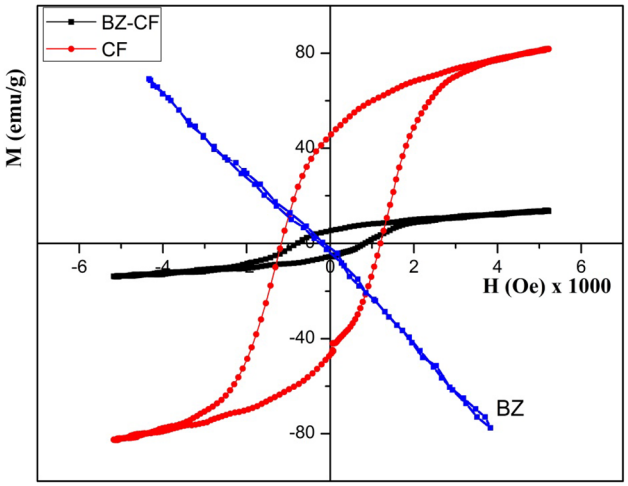

Fig. 7 Variation of magnetic hysteresis loops of pure BZ, CF nanoceramics, and BZ–CF nanocomposite at room temperature

Table 3 Saturation magnetization (M_s), remanence magnetization (M_r), coercivity (H_c), remanence ratio (M_r/M_s), and calculated magneton number (n_B) of BZ, CF nanoceramics, and BZ–CF nanocomposite

Sample	M_s (emu/g)	M_r (emu/g)	H_c (Oe)	M_r/M_s	n_B (μ_B)
BZ	–	–	–	–	–
CF	81.86	77.41	1172.3	0.95	3.43
BZ–CF	13.88	8.49	809.5	0.61	0.68

parameters such as saturation magnetization (M_s) and remanence magnetization (M_r) values are given in Table 3. The values of magnetic parameters of pure CF nanoparticles were in reported range [47].

From Table 3, it is observed that the magnetic parameters decrease for BZ–CF nanocomposite. Meanwhile, there are no hints of any interaction between the Fe^{3+} and Zr^{4+} ions, the influence due to coupling of spins between these can be excluded. The decrease in saturation magnetization values can be attributed to the reduced quantity of magnetic material per unit mass and the influence of $BaZrO_3$ and $BaCO_3$ diamagnetic phases. Similarly, as the magnetic nanoparticles are doped in diamagnetic matrix, a blockade is established between the external field and the magnetic material, thus decreasing the induced magnetization in the nanocomposite. The literature reveals that similar outcomes were obtained for cobalt ferrite nanoparticles dispersed in silica matrix [48].

A sharp decline in saturation magnetization from 81.86 to 13.88 emu/g was observed with combination of BZ nanoceramics indicating that the magnetic properties can be tuned by changing the BZ–CF ratio.

The Eq. (2) was used to calculate the experimental magnetization in Bohr magneton number unit [49]

$$n_B = \frac{(\text{mol.weight} \times M_s)}{5585}, \tag{2}$$

where M_s is saturation magnetization and N is Avogadro's number. The value of the magneton number of BZ–CF nanocomposite was lesser than pure CF sample.

Conclusions

The nanocomposite of $0.5(BaZrO_3)$–$0.5(CoFe_2O_4)$ (BZ–CF) was successfully synthesized via sol–gel autocombustion and mixing technique. The structural, microstructural, and magnetic properties of BZ, CF nanoceramics, and BZ–CF nanocomposite have been systematically investigated by XRD, FESEM, TEM, EDX, FTIR, and pulse field hysteresis loop tracer techniques. The BZ–CF nanocomposite shows the mixed phase of simple cubic perovskite and spinel structure. The average crystallite size calculated by Scherrer's formula confirms the nanocrystalline nature of the prepared samples. The lattice parameter and other structural parameter of the pure ceramics were in the reported range and that of BZ–CF nanocomposite was as expected. The average grain size determined from FESEM technique is of the order of 47–92 nm. The nanocrystillinity of the nanocomposite was confirmed from TEM analysis which confirms the production of spherical particles with mean diameter of ~ 36 nm. This EDX results indicate that the prepared samples of BZ, CF, and BZ–CF are pure without any impurity. The FTIR spectroscopic studies carried out show shifting of band frequencies which reflects the structural changes in BZ–CF nanocomposite. The FTIR spectrum of BZ shows a major band near 563 cm^{-1} and that of CF shows two prominent bands around 447 cm^{-1} and 696 cm^{-1} which are in reported range. The BZ–CF nanocomposite exhibits weak ferromagnetism while pure cobalt ferrite shows typical ferromagnetic nature. A sharp decline in saturation magnetization from 81.86 to 13.88 emu/g was observed with the combination of BZ nanoceramics indicating that the magnetic properties can be tuned by varying the BZ–CF ratio. The obtained material can be suitable for fabrication of spintronics and microwave devices.

Acknowledgements The author Dr. Pankaj P. Khirade is very much grateful to Department of Physics, IIT Mumbai for providing X-ray diffraction (XRD) and transmission electron microscopy (TEM), North Maharashtra University, Jalgaon for scanning electron microscopy (FESEM) research facilities.

References

1. Hull, D., Clyne, T.W.: An introduction to composite materials. Cambridge University Press, Cambridge (1996)
2. Khirade, P.P., Birajdar, S.D., Raut, A., Jadhav, K.: Multiferroic iron doped $BaTiO_3$ nanoceramics synthesized by sol–gel auto combustion: influence of iron on physical properties. Ceram. Int. **42**, 12441–12451 (2016)
3. Sanpo, N., Wen, C., Berndt, C.C., Wang, J.: Multifunctional spinel ferrite nanoparticles for biomedical application. Adv. Funct. Mater. **2015**, 183–217 (2015)
4. Rondinelli, J.M., May, S.J., Freeland, J.W.: Control of octahedral connectivity in perovskite oxide heterostructures: an emerging route to multifunctional materials discovery. MRS Bull. **37**, 261–270 (2012)
5. Sapate, D., Kale, C., Pandit, A., Jadhav, K.: Structural, magnetic and magnetoelectric properties of the magnetoelectric composite material. J. Mater. Sci. Mater. El. **25**, 3659–3663 (2014)
6. Testino, A., et al.: Preparation of multiferroic composites of BaTiO3–Ni0.5Zn0.5Fe2O4 ceramics. J. Eur. Ceram. Soc. **26**, 3031–3036 (2006)
7. Dimos, D., Mueller, C.: Perovskite thin films for high-frequency capacitor applications. Annu. Rev. Mater. Sci. **28**, 397–419 (1998)
8. Ishihara, T.: Perovskite oxide for solid oxide fuel cells. Springer, Berlin (2009)
9. Tressler, J.F., Howarth, T.R., Huang, D.: A comparison of the underwater acoustic performance of single crystal versus piezoelectric ceramic-based "cymbal" projectors. J. Acoust. Soc. Am. **119**, 879–889 (2006)
10. Bibes, M., Barthélémy, A.: Multiferroics: towards a magnetoelectric memory. Nat. Mater. **7**, 425 (2008)
11. Galasso, F.S.: Structure, properties and preparation of perovskite-type compounds: international series of monographs in solid state physics. Elsevier, Amsterdam (2013)
12. Gao, D., Guo, R.: Structural and electrochemical properties of yttrium-doped barium zirconate by addition of CuO. J. Alloys Compd. **493**, 288–293 (2010)
13. Khirade, P.P., Birajdar, S.D., Humbe, A.V., Jadhav, K.: Structural, electrical and dielectrical property investigations of Fe-doped $BaZrO_3$ nanoceramics. J. Electron. Mater. **45**, 3227–3235 (2016)
14. Sanchez, L.E., McDonald, A.J.: Preparation of sputtering targets. Google Patents, Mountain View (1998)
15. Farooq, M., Rita, R.A., Rossnagel, S.M.: Method for forming a perovskite thin film using a sputtering method with a fully oxidized perovskite target. Google Patents, Mountain View (2001)
16. Parida, S., et al.: Structural refinement, optical and microwave dielectric properties of BaZrO3. Ceram. Int. **38**, 2129–2138 (2012)
17. Ali, W.F.F.W., Rejab, N.A., Othman, M., Ain, M.F., Ahmad, Z.A.: An investigation of dielectric resonator antenna produced from silicon (100) enhanced by strontium doped-barium zirconate films. J. Solgel Sci. Technol. **61**, 411–420 (2012)
18. Mathew, D.S., Juang, R.-S.: An overview of the structure and magnetism of spinel ferrite nanoparticles and their synthesis in microemulsions. Chem. Eng. J. **129**, 51–65 (2007)
19. O'handley, R.C.: Soft magnetic materials. Mod Magn Mater **29**, 198 (2000)
20. Song, N., et al.: Facile synthesis and high-frequency performance of $CoFe_2O_4$ nanocubes with different size. J. Magn. Magn. Mater. **451**, 793–798 (2018)
21. Vinayak, V., Khirade, P.P., Birajdar, S.D., Alange, R., Jadhav, K.: Electrical and dielectrical properties of low-temperature-synthesized nanocrystalline Mg^{2+}-substituted cobalt spinel ferrite. J. Supercond. Nov. Magn. **28**, 3351–3356 (2015)
22. Amiri, S., Shokrollahi, H.: The role of cobalt ferrite magnetic nanoparticles in medical science. Mater. Sci. Eng., C **33**, 1–8 (2013)
23. Ding, Y., et al.: Single-walled carbon nanotubes wrapped $CoFe_2O_4$ nanorods with enriched oxygen vacancies for efficient overall water splitting. ACS Appl. Energy Mater. **2**, 1026–1032 (2018)
24. Lin, Y.-S., et al.: Multifunctional composite nanoparticles: magnetic, luminescent, and mesoporous. Chem. Mater. **18**, 5170–5172 (2006)
25. Kim, P., et al.: High energy density nanocomposites based on surface-modified BaTiO3 and a ferroelectric polymer. ACS Nano **3**, 2581–2592 (2009)
26. Kumar, A.S., et al.: Multiferroic and magnetoelectric properties of Ba0.85Ca0.15Zr0. 1Ti0. 9O3–$CoFe_2O_4$ core–shell nanocomposite. J. Magn. Magn. Mater. **418**, 294–299 (2016)
27. Kanakadurga, M., Raju, P., Murthy, S.R.: Preparation and characterization of $BaTiO3 + MgCuZnFe_2O_4$ nanocomposites. J. Magn. Magn. Mater. **341**, 112–117 (2013)
28. Liu, Y., et al.: Gram-scale synthesis of graphene quantum dots from single carbon atoms growth via energetic material deflagration. Chem. Mater. **27**, 4319–4327 (2015)
29. Vestal, C.R., Zhang, Z.J.: Synthesis and magnetic characterization of Mn and Co spinel ferrite-silica nanoparticles with tunable magnetic core. Nano Lett. **3**, 1739–1743 (2003)
30. Nitta, A., Nakamura, H., Komatsu, T., Matusita, K.: Interface reactions between silicon dioxide-lead oxide glass and manganese zinc ferrite. J. Am. Ceram. Soc. **72**, 1351–1354 (1989)
31. Paterson, J., Devine, R., Phelps, A.: Complex permeability of soft magnetic ferrite/polyester resin composites at frequencies above 1 MHz. J. Magn. Magn. Mater. **196**, 394–396 (1999)
32. Bayrakdar, H.: Complex permittivity, complex permeability and microwave absorption properties of ferrite–paraffin polymer composites. J. Magn. Magn. Mater. **323**, 1882–1885 (2011)
33. Khirade, P.P., Birajdar, S.D., Raut, A., Jadhav, K.: Effect of Fe–substitution on phase transformation, optical, electrical and dielectrical properties of BaTiO3 nanoceramics synthesized by sol–gel auto combustion method. J. Electroceram. **37**, 110–120 (2016)
34. Kanie, K., Seino, Y., Matsubara, M., Nakaya, M., Muramatsu, A.: Hydrothermal synthesis of $BaZrO_3$ fine particles controlled in size and shape and fluorescence behavior by europium doping. New J. Chem. **38**, 3548–3555 (2014)
35. Macario, L.R., Moreira, M.L., Andres, J., Longo, E.: An efficient microwave-assisted hydrothermal synthesis of $BaZrO_3$ microcrystals: growth mechanism and photoluminescence emissions. CrystEngComm **12**, 3612–3619 (2010)
36. Raut, A., Barkule, R., Shengule, D., Jadhav, K.: Synthesis, structural investigation and magnetic properties of Zn^{2+} substituted cobalt ferrite nanoparticles prepared by the sol–gel auto-combustion technique. J. Magn. Magn. Mater. **358**, 87–92 (2014)
37. Vinayak, V., Khirade, P.P., Birajdar, S.D., Sable, D., Jadhav, K.: Structural, microstructural, and magnetic studies on magnesium (Mg^{2+})-substituted $CoFe_2O_4$ nanoparticles. J. Supercond. Nov. Magn. **29**, 1025–1032 (2016)
38. Goyal, A., Bansal, S., Kumar, V., Singh, J., Singhal, S.: Mn substituted cobalt ferrites [$CoMn_xFe_{2-x}O_4$ ($x = 0.0, 0.2, 0.4, 0.6, 0.8, 1.0$)]: as magnetically separable heterogeneous nanocatalyst for the reduction of nitrophenols. Appl. Surf. Sci. **324**, 877–889 (2015)
39. Khirade, P.P., Shinde, A., Raut, A., Birajdar, S.D., Jadhav, K.: Investigations on the synthesis, structural and microstructural characterizations of Ba1-x Sr x ZrO_3 nanoceramics. Ferroelectrics **504**, 216–229 (2016)

40. Yamanaka, S., et al.: Thermochemical and thermophysical properties of alkaline-earth perovskites. J. Nucl. Mater. **344**, 61–66 (2005)
41. Cullity, B.D.: Elements of X-ray Diffraction (2001)
42. Pornprasertsuk, R., Yuwapattanawong, C., Permkittikul, S., Tungtidtham, T.: Preparation of doped $BaZrO_3$ and $BaCeO_3$ from nanopowders. Int. J. Precis. Eng. Manuf. **13**, 1813–1819 (2012)
43. Ostos, C., et al.: Synthesis and characterization of A-site deficient rare-earth doped $BaZr_xTi_{1-x}O_3$ perovskite-type compounds. Sol. State Sci **11**, 1016–1022 (2009)
44. Waldron, R.: Infrared spectra of ferrites. Phys. Rev. **99**, 1727 (1955)
45. Kumar, H.P., et al.: Characterization and sintering of $BaZrO_3$ nanoparticles synthesized through a single-step combustion process. J. Alloys Compd. **458**, 528–531 (2008)
46. Khirade, P.P., Birajdar, S.D., Shinde, A., Jadhav, K.: Room temperature ferromagnetism and photoluminescence of multifunctional Fe doped $BaZrO_3$ nanoceramics. J. Alloys Compd. **691**, 287–298 (2017)
47. Jadhav, S.S., Shirsath, S.E., Patange, S.M., Jadhav, K.: Effect of Zn substitution on magnetic properties of nanocrystalline cobalt ferrite. J. Appl. Phys. **108**, 093920 (2010)
48. Bardapurkar, P.P., Shewale, S.S., Barde, N.P., Jadhav, K.M.: Structural, magnetic and catalytical properties of cobalt ferrite nanoparticles dispersed in silica matrix. Mater. Res. Express. **6**, 045055 (2019)
49. Toksha, B., Shirsath, S.E., Patange, S., Jadhav, K.: Structural investigations and magnetic properties of cobalt ferrite nanoparticles prepared by sol–gel auto combustion method. Sol. State Commun. **147**, 479–483 (2008)